Appl. Phys. B (2015) 118:327–331
DOI 10.1007/s00340-014-5994-8

Applied Physics B
Lasers and Optics

Influence of heat transfer on nodule height of microstructured silicon fabricated by femtosecond laser pulses

Yan Peng · XiangQian Chen · YunYan Zhou · Kun Luo · YiMing Zhu

Received: 26 August 2014 / Accepted: 18 December 2014 / Published online: 30 December 2014
© Springer-Verlag Berlin Heidelberg 2014

Abstract By experiments and theory, we investigate the influence of heat transfer across a gas–solid interface on the nodule height of microstructured silicon fabricated under femtosecond laser pulses. By changing the pressure of the vacuum system, a fast-changing spread in height is found. This is determined by the different heat-transfer flux across the gas–solid interface for different Knudsen-number regimes. Heat transfer affects the energy remaining in the bulk silicon, which determines nodule formation and corresponding height. The rate of change in the heat-transfer flux induces a negative rate of change in the nodule height. These results are important when optimizing the surface microstructure for silicon-based photoelectron devices.

A quasi-periodic array of sharp microsized conical structures forms when femtosecond laser pulses are irradiated on the silicon surface in an environment of sulfur-bearing gases [1, 2]. For this microstructured silicon (MS), the absorption of light can be more than 90 % over a wide range of wavelength from 0.25 to 16.7 µm [3–6]. For its unique absorption properties, this material has attracted much interest with respect to its underlying mechanism and device applications [7–16]. Meanwhile, researchers have found that the sulfur-containing material creates many problems: First, after the necessary thermal treatment in the semiconductor fabrication process (e.g., ohmic contact formation and deactivation), the broadband optical absorption capability drops off rapidly. Second, after various high-temperature processes, the optically active state of sulfur impurities in bulk silicon becomes inactive [17] and acts as a recombination center that can capture photoexcited carriers, thereby decreasing the photocurrent of the device. These problems can greatly reduce the efficiency of optoelectronic devices that employ MS.

To mitigate these problems, researchers have tried to fabricate a similar material in vacuum [18–22]. The antireflection and absorption capacities of MS were then found to be mainly determined by the sharp conical structures (spikes) and doping concentration in the silicon substrate. Distinct from impurities doped during laser fabrication, infrared absorption contributed by the impurities (such as phosphor) in the silicon substrate is not affected by the high-temperature process. Additionally, for MS, incident light undergoes multiple reflections between spikes, which can then increase the infrared absorption from doped impurities. Hence, taller spikes on MS surfaces are beneficial for improving the antireflection and optical absorption capacity of the MS material. Nevertheless, few studies, especially with quantified analyses, exist on controlling height of MS under vacuum conditions.

In this paper, combining the results from the analysis of heat transfer across a gas–solid interface, we demonstrate that within the same pressure range, the fast-changing heat-transfer flux within different Knudsen-number regimes can induce significant changes in height. The treatment can yield tall conical spikes under specific vacuum conditions. These results are important for extending the range of applications of MS in semiconductor devices.

Y. Peng · X. Chen · Y. Zhou · K. Luo · Y. Zhu (✉)
Shanghai Key Lab of Modern Optical System, Engineering Research Center of Optical Instrument and System Ministry of Education, University of Shanghai for Science and Technology, No. 516 JunGong Rd., Shanghai 200093, China
e-mail: ymzhu@usst.edu.cn

Y. Peng
The Institute of Optics, University of Rochester, Rochester, NY 14627, USA

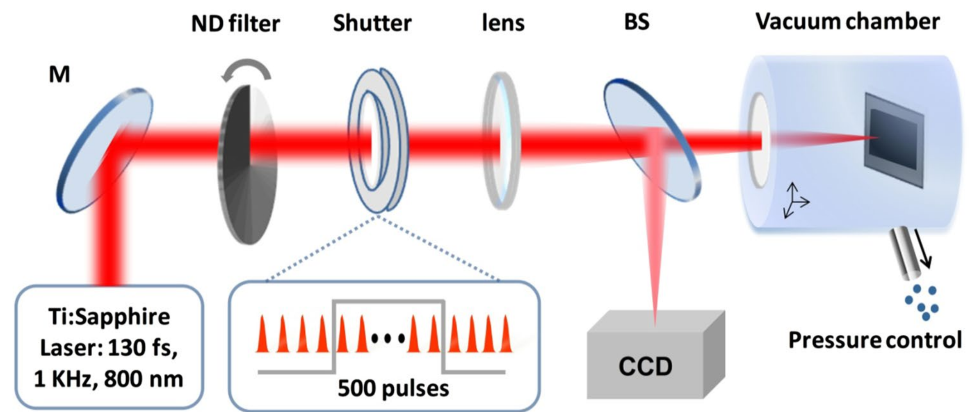

Fig. 1 Schematic of the experimental setup to microstructure the surface of silicon wafers. M: mirror with a coating of HR@800 nm; BS: beam splitter with a 1:10 splitting ratio; *ND* neutral density

We subjected silicon surfaces to a femtosecond-pulsed laser beam under different vacuum pressures. With our experimental setup (Fig. 1), laser pulses were produced using a Ti: sapphire regenerative amplifier, typically 800 nm, 1 kHz, and 130 fs. The intensity of the incident laser beam was adjusted using a circular variable metallic neutral-density filter; the pulse number was controlled by a beam shutter (here, the single pulse energy and the pulse number were set at 0.6 mJ and 500, respectively). The laser beam was focused with a convex lens ($f = 1$ m) and directed into the chamber through a quartz window of 0.4 mm thickness. A silicon wafer (phosphor-doped *n*-type silicon wafer, resistivity: 0.01–0.02 Ω cm) was mounted in the vacuum chamber with its (100) face oriented vertically toward the direction of the laser beam. Using a beam splitter in front of the vacuum chamber, a part of the light beam was reflected into a CCD beam profiler, which enabled the laser spot on the sample surface to be monitored in real time (the diameter of the laser spot was about 300 μm).

In our experiments, the vacuum pressure was varied from 5×10^{-2} to 3×10^{4} Pa (the vacuum system determined the pressure range). After fabrication, the surface morphology of the MS was evaluated using scanning electron microscopy (SEM); typical images are shown in Fig. 2.

As vacuum pressure gradually increases, the microstructures forming on the silicon surfaces (Fig. 2) changed from sharp cones to blunt nodules. The average height of the microstructures gradually decreases. For clarity, we present data of their average height under the different vacuum pressures (Fig. 3a). Measurements of the height were obtained using the SEM images and taking the distance from the top to the bottom of a microstructure and dividing by the cosine of the viewing angle. The measuring error is ~1 μm. The final values given for the average height are averaged over five measurements taken at the same vacuum pressure. We see that the average height rapidly declines over the pressure range from 1×10^{2} to 3×10^{4} Pa. Considering that nodule formation is directly determined by the energy absorbed and retained by the bulk silicon [23, 24] and that the beam energy is always the same, we therefore hypothesize that the rapid change in height results from a heat transfer across the air–silicon surface and energy losses in the vacuum system. Hence, we first analyze the heat transfer across a gas–solid interface under different pressures.

The heat-transfer process can be divided into four distinct regimes [25, 26] that are characterized by numerical values assigned to the Knudsen-number Kn. This number is defined as the ratio of the mean free path λ of molecules to a characteristic length d that is usually taken to be the gas-layer thickness, i.e.,

$$Kn = \frac{\lambda}{d}, \tag{1}$$

with

$$\lambda = \frac{KT}{\sqrt{2}P\pi\varphi^2}, \tag{2}$$

where $K = 1.380 \times 10^{-23}$ J K^{-1} is Boltzmann's constant, T the effective gas temperature, P the gas pressure, and φ the average diameter of the gas molecules (for air: $\varphi = 4.0 \times 10^{-10}$ m).

The four different heat-transfer regimes are: the continuum regime ($Kn < 0.001$), temperature-jump regime ($0.001 < Kn < 0.1$), transition regime ($0.1 < Kn < 10$), and free-molecule regime ($Kn > 10$). Here, parallel-plate geometry is used to calculate the heat transfer, where the stationary air is contained between two silicon plates. Considering that the heat transfer in the near-field (the region within 100 nm from a solid interface) is several orders of magnitude higher than that in the far-field [27, 28] and that the MS is a material with a high surface-to-volume ratio, the active region in heat transfer is near the nodules. Therefore, their average height for a given pressure is considered a characteristic length and was used in our heat-transfer calculations. This assumption prescribes that the range in vacuum pressure in our experiments covers three heat-transfer

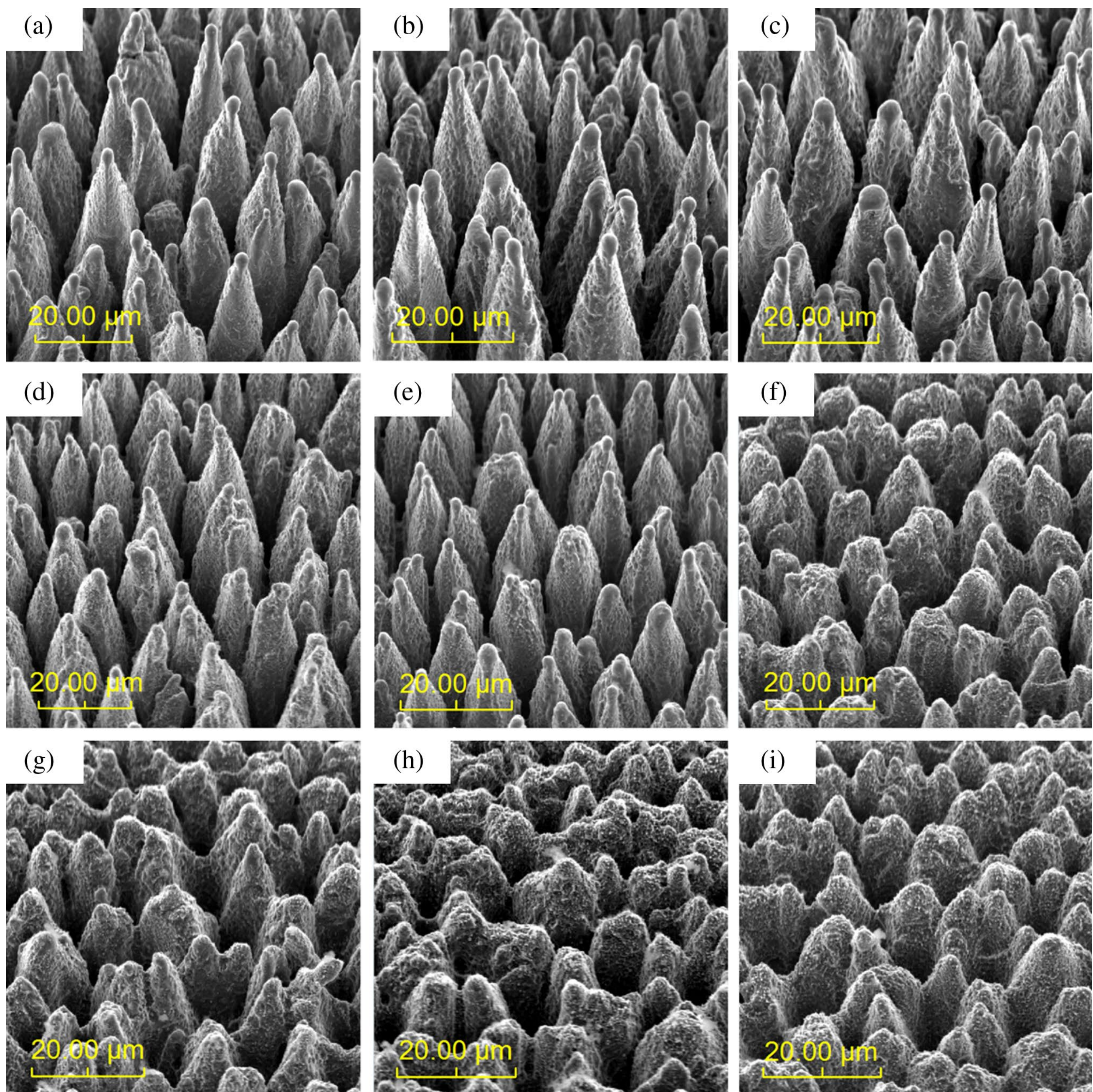

Fig. 2 SEM images of microstructured silicon after femtosecond laser irradiation under different vacuum pressures: **a** 10^{-1}, **b** 10^{1}, **c** 10^{2}, **d** 2×10^{3}, **e** 3×10^{3}, **f** 4×10^{3}, **g** 5×10^{3}, **h** 10^{4}, **i** 2×10^{4} Pa. The viewing angle is 45° from the surface normal

regimes—free-molecule, transition, and temperature-jump, labeled I, II, and III, respectively, in Fig. 3a. Three different formulas for the heat flux are then used [25, 26]:

I. for the free-molecule heat-conduction regime

$$Q_{\mathrm{FM}} = \left(\frac{1}{\alpha_1} + \frac{1}{\alpha_2} - 1\right)^{-1} \frac{P\left(C_{\mathrm{v}} + \frac{R}{2}\right)}{\left(2\pi RTM_{\mathrm{g}}\right)^{\frac{1}{2}}}(T_1 - T_2), \quad (1)$$

where $\alpha_1 = \alpha_2 = 0.82$ are the thermal accommodation coefficients of silicon surfaces [29], $C_{\mathrm{v}} = 20.801$ J K^{-1} mol^{-1} is the molar heat capacity of air at constant volume, $R = 8.314$ J K^{-1} mol^{-1} is the molar gas constant of air, $M_{\mathrm{g}} = 28.966$ g mol^{-1} is the molecular weight of the air, $T_1 = 373$ K and $T_2 = 298$ K are the temperatures of the silicon surfaces for irradiated and un-irradiated area, respectively [$T = (T_1 + T_2)/2 = 335.5$ K].

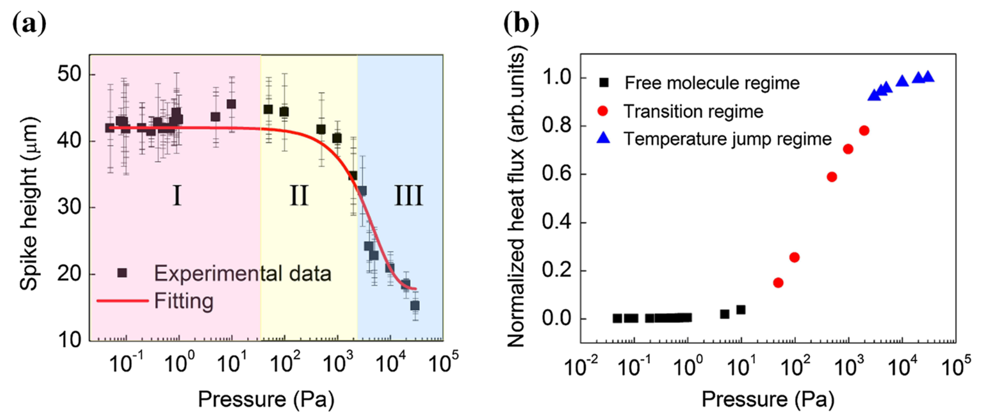

Fig. 3 **a** Average height of microstructures as a function of vacuum pressure. *Squares* denote experimental data; *red solid line* is the fitted curve. Associated *error bars* are also given. **b** Normalized heat flux across the gas–solid interface as a function of vacuum pressure. *Note* the log scale used for both abscissas

II. for the transition regime

$$Q_{\mathrm{TR}} = Q_{\mathrm{FM}}\left[1+\frac{4B}{15}\left(\frac{d}{\lambda}\right)\alpha_m\right]^{-1}. \tag{2}$$

Here, $B = 45/38$ and α_m can be obtained from the expression $\frac{\alpha_m}{2-\alpha_m} = \frac{\alpha_1-\alpha_2}{\alpha_2+\alpha_1(1-\alpha_2)}$.

III. for the temperature-jump regime:

$$Q_{\mathrm{TJ}} = Q_{\mathrm{FM}}\left\{\left(\frac{1}{\alpha_1}+\frac{1}{\alpha_2}-1\right)^{-1} \times\left[\frac{4B}{15}\left(\frac{d}{\lambda}\right)+\frac{1}{2}\left(\frac{2-\alpha_1}{\alpha_1}+\frac{2-\alpha_2}{\alpha_2}\right)\right]\right\}^{-1}. \tag{3}$$

Based on these parameters and formulas, we quantify the heat-transfer flux as a function of vacuum pressure (the calculated pressure values are in agreement with the experimental data). To make the comparison more clear, the calculated results are normalized and plotted in Fig. 3b with different symbols and colors according to the regime.

The heat-transfer flux is seen to change slowly when the pressure is low in the free-molecule regime. When the vacuum pressure enters the regions corresponding to the transition regime and temperature-jump regime, heat flux values change rapidly from almost 0 to 1. This indicates that the heat transfer across the air–silicon interface increases rapidly as the pressure increases. If heat transfers take typically ~1 ps, whereas the pulse duration of irradiated laser is of order ~1 fs, the entire period from energy deposition to the appearance of final structure is of order ~1 ns [30]; therefore, we infer that after beam energy is absorbed by the silicon material, the heat transfer between silicon and air begins to occur during nodule formation. The heat transfer decreases the energy retained in the bulk silicon, which dictates the energy available in nodule formation and hence their corresponding height. That is, the change in heat-transfer flux directly affects the final average height of the nodules.

Thus, the dependence of nodule formation on vacuum pressure can be explained: Under laser irradiation, the silicon wafer absorbs laser energy. When a sufficient amount of energy is absorbed, silicon begins to melt; capillary waves and ripples form a quasi-periodic array of beads that leads to the formation of nodules on the silicon surface [31]. For femtosecond laser pulses, if the single-pulse energy and pulse number are fixed, the beam energy that is effectively absorbed by bulk silicon in unit time is fixed [23, 24]. After the energy is absorbed, the degree of heat transfer at the air–silicon interface determines how much energy is retained within the bulk silicon. The more the energy remaining, the higher the temperature in the surface layer, resulting in more melting and ablation of silicon. Finally, the material melt and its ablation determine the nodule height that is obtained. Therefore, the lower the heat-transfer flux across the air–silicon interface, the more energy remains within the material, and hence, the higher the nodule height will be. In consequence, as the vacuum pressure increases, the rate of change in heat flux induces a negative correlation with the rate of change of average nodule heights (see Fig. 3a, b).

However, we notice that in Fig. 3, the rate of change in heat flux is not completely correlated with height. For example, for the temperature-jump regime, the rate of change in heat flux is slower than that of height, whereas for the transition regime, it is quicker. We believe these observations result from differences in energy loss in gas dissociation under different pressures. It is well known that under femtosecond laser irradiation, nitrogen and oxygen are easily dissociated after they absorb beam energy, and oxygen can react with silicon to form silicon oxide (in our experiments, the laser intensity 420 J/cm^2 is large enough for gas dissociation even under pressures of 10^5 Pa [32–34]). Additionally, the plasma formed from gas dissociation can defocus the laser beam, which also decreases the beam energy reaching the silicon layer [33]. Under low vacuum

pressure, the number of molecules is small, and therefore little energy is lost during these reactions. Moreover, as gas pressure increases, more irradiated laser energy is used in gas dissociation and chemical reactions. As a result, at the same irradiated beam energy, the energy loss increases rapidly with pressure, rapidly lowering the amount of energy absorbed by bulk silicon. Finally, the effective beam energy that remains for nodule formation decreases rapidly. Therefore, as pressure increases, even the rate of change in heat transfer slows; the fast-increasing energy losses cause nodule heights to decrease rapidly.

In summary, combining a quantified analysis of heat transfer across a gas–solid interface, we demonstrated by experiments the influence of heat transfer on the average height of nodules of laser-ablated silicon. Average heights are higher if heat transfer is lower and vice versa. Additionally, the dissociation of air caused by the femtosecond-pulsed laser beam also affects nodule formation. These results are meaningful for promoting the development of MS material fabrication for solar cell, sensors, photoelectron devices, and their interdisciplinary fields.

Acknowledgments This work was partly supported by National Natural Science Foundation of China (11104186, 61138001), Program of Shanghai Subject Chief Scientist (14XD1403000), Shanghai Basic Research Key Project (12JC1407100), “Chen Guang” Project of Shanghai Municipal Education Commission and Educational Development Foundation (12CG54), and State Scholarship Fund (201308310172).

References

1. R. Younkin, J.E. Carey, E. Mazur, J.A. Levinson, C.M. Friend, J. Appl. Phys. **93**, 2626 (2003)
2. M.A. Sheehy, L. Winston, J.E. Carey, C.M. Friend, E. Mazur, Chem. Mater. **17**, 3582 (2005)
3. T. Her, R.J. Finlay, C. Wu, S. Deliwala, E. Mazur, Appl. Phys. Lett. **73**, 1673 (1998)
4. Y. Peng, M. Hong, Y. Zhou, D. Fang, X. Chen, B. Cai, Y. Zhu, Appl. Phys. Express **6**, 051303 (2013)
5. J. Yang, Y. Yang, B. Zhao, Y. Wang, X. Zhu, Appl. Phys. B **106**, 349 (2012)
6. Y. Peng, D.S. Zhang, H.Y. Chen, Y. Wen, S.D. Luo, L. Chen, K.J. Chen, K.J. Chen, Y.M. Zhu, Appl. Opt. **51**, 635 (2012)
7. B.K. Nayak, V.V. Iyengar, M.C. Gupta, Prog. Photovolt. **19**, 631 (2011)
8. H.Y. Chen, G.D. Yuan, Y. Peng, M. Hong, Y.B. Zhang, Y. Zhang, Z.Q. Liu, J.X. Wang, B. Cai, Y.M. Zhu, J.M. Li, Appl. Phys. Lett. **104**, 193904 (2014)
9. H.M. Branz, V.E. Yost, S. Ward, K.M. Jones, B. To, P. Stradins, Appl. Phys. Lett. **94**, 231121 (2009)
10. S. Zhang, Y. Li, G. Feng, B. Zhu, S. Xiao, L. Zhou, L. Zhao, Opt. Express **19**, 20462 (2011)
11. H. Nakanishi, S. Fujiwara, K. Takayama, I. Kawayama, H. Murakami, M. Tonouchi, Appl. Phys. Express **5**, 112301 (2012)
12. P. Hoyer, M. Theuer, R. Beigang, E.-B. Kley, Appl. Phys. Lett. **93**, 091106 (2008)
13. V. Zorba, E. Stratakis, M. Barberoglou, E. Spanakis, P. Tzanetakis, S.H. Anastasiadis, C. Fotakis, Adv. Mater. **20**, 4049 (2008)
14. T. Baldacchini, J.E. Carey, M. Zhou, E. Mazur, Langmuir **22**, 4917 (2006)
15. H.R. Dehghanpour, P. Parvin, B. Sajad, S.S. Nour-Azar, Appl. Surf. Sci. **255**, 4664 (2009)
16. T.H. Her, R.J. Finlay, C. Wu, E. Mazur, Appl. Phys. A **70**, 383 (2000)
17. C.B. Simmons, A.J. Akey, J.J. Krich, J.T. Sullivan, D. Recht, M.J. Aziz, T. Buonassisi, J. Appl. Phys. **114**, 243514 (2013)
18. R. Torres, V. Vervisch, M. Halbwax, T. Sarnet, P. Delaporte, M. Sentis, J. Ferreira, D. Barakel, S. Bastide, F. Torregrosa, H. Etienne, L. Roux, J. Optoelectron. Adv. Mater. **12**, 621 (2010)
19. Y. Peng, X. Chen, Y. Zhou, G. Xu, B. Cai, J. Xu, R. Henderson, J. Dai, Y. Zhu, J. Appl. Phys. **116**, 073102 (2014)
20. P. Banerji, Appl. Surf. Sci. **253**, 5129 (2007)
21. S. Liu, J. Zhu, Y. Liu, L. Zhao, Mater. Lett. **62**, 3881 (2008)
22. S. Dannefaer, D. Kerr, C. Craigen, T. Bretagnon, T. Taliercio, A. Foucaran, J. Appl. Phys. **79**, 9110 (1996)
23. Y. Peng, Y. Wen, D. Zhang, S. Luo, L. Chen, Y. Zhu, Appl. Opt. **50**, 4765 (2011)
24. Y. Peng, H.Y. Chen, C.G. Zhu, D.S. Zhang, Y.Y. Zhou, H. Xiang, B. Cai, Y.M. Zhu, Mater. Lett. **83**, 127 (2012)
25. G.S. Springer, Heat transfer in rarefied gases, in *Advances in Heat Transfer*, vol. 7, Academic Press, ed. by J.P. Hartnett, T.F. Irvine Jr. (New York, NY, 1971), pp. 163–218
26. Y. Demirel, S.C. Saxena, Energy **21**, 99 (1996)
27. K.D. Kihm, *Near-Field Characterization of Micro/Nano-Scaled Fluid Flows* (Springer, Berlin, 2011)
28. C. Cheng, W. Fan, J. Cao, S. Ryu, J. Li, C.P. Grigoropoulos, J. Wu, ACS Nano **5**, 10102 (2011)
29. W.M. Trott, J.N. Castaneda, J.R. Torczynski, M.A. Gallis, D.J. Rader, Rev. Sci. Instrum. **82**, 035120 (2011)
30. D. von der Linde, K. Sokolowski-Tinten, J. Bialkowski, Appl. Surf. Sci. **109**, 1 (1997)
31. B.R. Tull, J.E. Carey, E. Mazur, J.P. Mcdonald, S.M. Yalisove, MRS Bull. **31**, 626 (2006)
32. J.H. Marburger, Prog. Quantum Electron. **4**, 35 (1975)
33. S.L. Chin, S.A. Hosseini, W. Liu, Q. Luo, F. Theberge, N. Aközbek, A. Becker, V.P. Kandidov, O.G. Kosareva, H. Schroeder, Can. J. Phys. **83**, 863 (2005)
34. A.Y. Vorobyev, C. Guo, Nat. Sci. **3**, 488 (2011)